University Library

MINERVA ACCESS

A gateway to Melbourne's research publications

Minerva Access is the Institutional Repository of The University of Melbourne

Author/s:
Baumgartner, RJ;Van Kranendonk, MJ;Fiorentini, ML;Pagès, A;Wacey, D;Kong, C;Saunders, M;Ryan, C

Title:
Formation of micro-spherulitic barite in association with organic matter within sulfidized stromatolites of the 3.48 billion-year-old Dresser Formation, Pilbara Craton

Date:
2020-07-01

Citation:
Baumgartner, R. J., Van Kranendonk, M. J., Fiorentini, M. L., Pagès, A., Wacey, D., Kong, C., Saunders, M. & Ryan, C. (2020). Formation of micro-spherulitic barite in association with organic matter within sulfidized stromatolites of the 3.48 billion-year-old Dresser Formation, Pilbara Craton. Geobiology, 18 (4), pp.415-425. https://doi.org/10.1111/gbi.12392.

Persistent Link:
https://hdl.handle.net/11343/275708

Check for updates

Formation of micro–spherulitic barite in association with organic matter within sulfidized stromatolites of the 3.48 billion–year–old Dresser Formation, Pilbara Craton

Author Manuscript

Authors

Raphael J. Baumgartner[1], Martin J. Van Kranendonk[1], Marco L. Fiorentini[2], Anais Pages[3], David Wacey[4], Charlie Kong[5], Martin Saunders[4], Chris Ryan[6]

[1]School of Biological, Earth and Environmental Sciences, The University of New South Wales, Kensington, New South Wales 2052, Australia.

[2]School of Earth Sciences, The University of Western Australia, Perth, Western Australia 6009, Australia.

[3]Commonwealth Scientific and Industrial Research Organization, Mineral Resources, Kensington, Western Australia 6151, Australia.

[4]Centre for Microscopy, Characterization and Analysis, The University of Western Australia, Perth, Western Australia 6009, Australia.

[5]Electron Microscopy Unit, The University of New South Wales, Kensington, New South Wales 2052, Australia.

[6]Commonwealth Scientific and Industrial Research Organization, Mineral Resources, Melbourne, Victoria 3168, Australia

*Corresponding author (r.baumgartner@unsw.edu.au; raphael-johannes.baumgartner@hotmail.com)

Author contributions

The methodology was conceived by R.J. Baumgartner, M.J. Van Kranendonk, and M.L. Fiorentini. All analytical work was carried out by R.J. Baumgartner, with assistance by D. Wacey and M. Saunders (Focused Ion Beam Milling and Transmission Electron Microscopy), as well as A. Pages

This is the author manuscript accepted for publication and has undergone full peer review but has not been through the copyediting, typesetting, pagination and proofreading process, which may lead to differences between this version and the Version of Record. Please cite this article as doi: 10.1111/GBI.12392

This article is protected by copyright. All rights reserved

and C. Ryan (Scanning Electron Microscopy and/or Synchrotron Radiation X–ray Fluorescence Microscopy). The manuscript was written by R.J. Baumgartner, with input from all co–authors.

Author Manuscript

ACKNOWLEDGEMENTS

The authors acknowledge the facilities, and the scientific and technical assistance of the Microscopy Australia research facility at the Centre for Microscopy, Characterization and Analysis (UWA). This study was supported by the Australian Research Council (ARC) Centre of Excellence for Core to Crust Fluid Systems (www.ccfs.mq.edu.au). Additional support came from the University of New South Wales (Sydney), and ARC Discovery Project 180103204.

This article is protected by copyright. All rights reserved

Formation of micro–spherulitic barite in association with organic matter within sulfidized stromatolites of the 3.48 billion–year–old Dresser Formation, Pilbara Craton

ABSTRACT

The shallow marine and subaerial sedimentary and hydrothermal rocks of the ~3.48 billion–year–old Dresser Formation are host to some of Earth's oldest stromatolites and microbial remains. This study reports on texturally distinctive, spherulitic barite micro–mineralization that occur in association with primary, autochthonous organic matter within exceptionally preserved, strongly sulfidized stromatolite samples obtained from drill cores.

Spherulitic barite micro–mineralization within the Dresser Formation sulfidized stromatolites generally forms submicron–scale aggregates that show gradations from hollow to densely crystallized, irregular to partially radiating crystalline interiors. Several barite micro–spherulites show thin outer shells. Within stromatolites, barite micro–spherulites are intimately associated with petrographically earliest dolomite and nano–porous pyrite enriched in organic matter, the latter of which is a possible biosignature assemblage that hosts microbial remains. However, barite spherulites are also observed within layered barite in proximity to stromatolite layers, where they are overgrown by compositionally distinct (Sr–rich), coarsely crystalline barite that may have been sourced from hydrothermal veins at depth.

Micro–spherulitic barite, such as reported here, is not known from hydrothermal systems that exceed the upper temperature limit for life. Rather, barite with near–identical morphology and micro–texture is known from zones of high bio–productivity under low–temperature conditions in the modern oceans, where microbial activity and/or organic matter of degrading biomass controls the formation of spherulitic aggregates. Hence, the presence of micro–spherulitic barite in the organic matter–bearing Dresser Formation sulfidized stromatolites lends further support for a biogenic origin of these unusual, exceptionally well–preserved, and very ancient microbialites.

KEY WORDS

Spherulitic barite, Paleoarchean, Dresser Formation, Stromatolites, Organic matter

INTRODUCTION

The ~3.48 Ga Dresser Formation in the North Pole Dome of the East Pilbara Terrane (Western Australia) is famous for hosting exceptional evidence for some of Earth's oldest life. Stromatolites are widespread and common in the North Pole Chert Member of the Dresser Formation, where they occur within shallow water to subaerial deposits that have been variably influenced by circulating hydrothermal fluids (Walter et al., 1980; Groves et al., 1981; Van Kranendonk, 2006, 2011; Van

This article is protected by copyright. All rights reserved

Author Manuscript

Kranendonk et al., 2008; Djokic et al., 2017; Baumgartner et al., 2019, 2020a). A biological origin of these stromatolites is demonstrated by a diverse array of textural features that are indicative of microbially mediated formation (Walter et al., 1980; Buick et al., 1981; Van Kranendonk et al., 2008; Baumgartner et al., 2019; among others), and by the presence of associated organic matter, including potential microbial remains, whose syngenetic origin is demonstrated by relationships with stromatolite geometry and primary mineralogy (Baumgartner et al., 2019). Additional support for ancient life in the Dresser Formation includes: i) organic matter and methane–rich fluid inclusions in quartz of bedded and hydrothermal vein chert, which show carbon isotope signatures that are expected for biological formation (Ueno et al., 2001, 2006; Morag et al., 2016; Duda et al., 2018); iii) sulfur isotope signatures of pyrite mineralization that match the isotopical fractionation trends expected for sulfur–cycling organisms, notably microbes dependent on sulfate reduction and/or disproportionation of elemental sulfur (Shen et al, 2001, 2009; Philippot et al., 2007; Ueno et al., 2008; Baumgartner et al., 2020b).

The Dresser Formation also hosts large barite deposits that occur in a dense network of hydrothermal veins, and in laterally extensive, coarse–grained barite layers within bedded cherts (Buick and Dunlop, 1990; Nijman et al., 1998; Van Kranendonk et al., 2001, 2008; Pirajno and Van Kranendonk, 2004). The bedding–parallel barite deposits were originally interpreted as replacive mineralization, formed after gypsum evaporites that precipitated in a restricted lagoon setting (Buick and Dunlop et al., 1990). However, the recognition of barite as a primary precipitate, and that the bedding–parallel, coarse–grained barite has intrusive relationships with the host sedimentary rocks, indicate that it precipitated from circulating and venting hydrothermal fluids in a low–eruptive volcanic caldera setting (Nijman et al., 1998; Runnegar et al., 2001; Van Kranendonk and Pirajno, 2004; Van Kranendonk, 2006; Van Kranendonk et al., 2008). In this scenario, Ba^{2+} is interpreted to have been sourced mainly from footwall basalts through leaching by hydrothermal fluids, whereas SO_4^{2-} could have been derived from both the hydrothermal systems and intermixed seawater (Nijman et al., 1998; Van Kranendonk et al., 2001; Van Kranendonk and Pirajno, 2004; Van Kranendonk, 2006; Ueno et al., 2008; Shen et al., 2009; Philippot et al., 2012; Baumgartner et al., 2020b).

Here, we report the discovery of micro–spherulitic barite within exceptionally preserved Dresser Formation sulfidized stromatolites from unweathered drill core samples (Kranendonk et al., 2008). These texturally distinctive barite micro–mineralization occur in two associations: 1) as agglomerations in association with organic matter (including microbial remains; c.f., Baumgartner et al., 2019) that are preserved within petrographically earliest dolomite and nano–porous pyrite of the sulfidized stromatolites; 2) as agglomerations within coarse–grained, compositionally distinct (Sr–rich) barite crystals that grew in beds between horizons of the sulfidized stromatolites. Micro–spherulitic

This article is protected by copyright. All rights reserved

Author Manuscript

barite very similar to that in this study is known to form under low–temperature marine conditions in the presence of microbial activity and/or derived organic matter (e.g., González–Muñoz et al., 2003, 2012; Smith et al., 2004; Stevens et al., 2015; Torres–Crespo et al., 2015). Hence, micro–spherulitic barite within the 3.48 billion–year–old Dresser Formation sulfidized stromatolites supports a biological origin for these ancient, exceptionally–preserved microbialites.

GEOLOGICAL BACKGROUND AND SETTING OF STROMATOLITE GROWTH

The 3481 ± 2 Ma Dresser Formation of the Warrawoona Group is located in the North Pole Dome of the East Pilbara Terrane, Western Australia (Fig. 1a; Van Kranendonk et al., 2007). A wide variety of stromatolites occur within the North Pole Chert Member at the base of the Dresser Formation, which is a thin (~ 2–120 m) hydrothermal–sedimentary succession composed of interbedded, white–grey–black chert, thick layers of coarsely crystalline barite, silicified sandstone and conglomerate, carbonates, siliceous hot spring sinter deposits, and jaspilitic chert (Walter et al., 1980; Groves et al., 1981; Van Kranendonk, 2006, 2011; Van Kranendonk et al., 2008; Djokic et al., 2017). Stromatolites are strongly weathered in surface outcrops, but were found to consist predominately of pyrite and dolomite in unweathered drill cores (Van Kranendonk et al., 2008). The Dresser Formation has been metamorphosed under prehnite-pumpellyite to lower greenschist facies conditions (Dunlop and Buick, 1981; Terabayashi et al., 2003).

The interpretation for a hydrothermally influenced depositional setting of stromatolite growth is supported by the recognition of syngenicity between emplacement of the Dresser Formation and underlying swarms of hydrothermal chert–barite veins (Nijman et al., 1998; Van Kranendonk and Pirajno, 2004). This is demonstrated by the fact that hydrothermal veins transect basal basalt and komatiitic basalt but terminate within the North Pole Chert Member of the Dresser Formation, and that clasts of hydrothermal, coarse–grained barite occur in sandstones and conglomerates of the North Pole Chert Member (Van Kranendonk and Pirajno, 2004; Van Kranendonk, 2006). Hence, the growth of stromatolites has likely occurred in proximity to, and perhaps was directly linked with, shallow marine to subaerial venting of hydrothermal fluids within a closed, evaporitic to subaerial volcanic caldera basin (Van Kranendonk 2006; Van Kranendonk et al., 2008; Djokic et al., 2017).

MATERIALS AND METHODS

The stromatolite samples examined in this study are derived from ~ 89 m depth in a fresh diamond drill core (Pilbara Drilling project; PDP) that was obtained from the North Pole Chert Member of the Dresser Formation (Fig. 1b; Philippot et al., 2007; Van Kranendonk et al., 2008). Details on the stratigraphy of the drill core, spatial correlation with stromatolites in surface outcrops, and inferences on the geological context of stromatolite formation, are reported in Van Kranendonk et

This article is protected by copyright. All rights reserved

Author Manuscript

al. (2008). The microtextures, mineralogy, and chemistry of the drill core stromatolites samples are documented in Baumgartner et al. (2019, 2020a). One polished thin section and two polished epoxy mounts that were prepared in the study of Baumgartner et al. (2019) from centimeter–sized rock slabs taken from the centre of the drill cores were examined in detail for contained barite mineralization.

Synchrotron Radiation X–ray Fluorescence Microscopy (SR–XFM)

Element mapping by SR–XFM was performed on polished epoxy mounts at the XFM beamline at the Australian Synchrotron in Melbourne. Parts of the acquired SR–XFM data were already reported in Baumgartner et al. (2020a). The beam was focused using the Kirkpatrick Baez mirror microprobe end–station, which resulted in a monochromatic 2 µm beam with energies in the range 4 – 20 keV. The XFM beamline is equipped with the high solid–angle, energy–dispersive multi–element detector MAIA, which allows for element mapping of large areas with ~ 2 µm² resolution (Paterson et al., 2011). Spectral maps were acquired over areas of several square centimetres using count rates of 4 –10 M/s. The energy resolution was 0.3 – 0.4 keV. The spectral maps were processed using GeoPIXE (CSIRO) into element concentrations by standardless correction of the raw data (Ryan et al., 2010). The results are presented as tricolour (red, green and blue) multi–element maps.

Scanning Electron Microscopy (SEM)

Backscattered Electron imagery and Energy Dispersive X–ray Spectroscopy analysis was performed using a FEI XHR–Verios 460L field–emission SEM at the Centre for Microscopy, Characterisation and Analysis (CMCA), University of Western Australia (UWA). The analytical setup involved 3 – 20 kV acceleration voltage and 0.1 – 0.8 nA beam current for imaging, whereas up to 15 kV and 0.8 – 1.6 nA was used for EDS analysis. Both the electron imagery and chemical analysis were done without the use of conductive coatings. Elements were determined using characteristic Kα and Kβ X–ray emission lines.

Nitric–acid etching

Following initial textural, mineralogical and chemical examination, the epoxy mounts were ground and repolished, cleaned with ethanol and distilled water, and then etched for ~ 60 – 90 s with 70 % nitric acid (HNO_3). After rinsing with distilled water and air–drying in an exicator, the exposed organic matter and mineralogy were analyzed and imaged by Raman Spectroscopy and SEM–EDS analysis.

Focused ion beam (FIB) milling and Scanning Transmitted Electron Microscopy (STEM)

A STEM wafer of micro–spherulitic barite was prepared from nitric acid–etched sample material using a FEI Helios NanoLab G3 CX DualBeam FIB–SEM (installed at CMCA, UWA). Preparation involved deposition of a thick protective Pt layer, following which the ultrathin wafer was

This article is protected by copyright. All rights reserved

Author Manuscript

milled to a thickness of ~ 150 nm using a Ga ion beam. Bright– and dark–field STEM imagery was performed at CMCA, UWA, using a FEI Titan G2 80–200 TEM/STEM with ChemiSTEM Technology operated at 200 kV. Element maps were obtained by EDS with a Super–X detector using a probe size of ~ 1 nm and a probe current of ~ 0.9 nA. Elements were determined using characteristic Kα and Kβ X–ray emission lines. The EDS maps were produced using ESPRIT 2 (Bruker Corporation).

Raman Spectroscopy (RS)

Raman Spectroscopy analysis of organic matter that occurs in association with micro–spherulitic barite was carried out at CMCA, UWA, using a WITec alpha 300RA+ Raman probe combined with a peltier–cooled 1024 × 1280 pixel CCD detector, and a Toptica Photonics Xtra II 785 nm laser source. A 50x/0.9 objective was used for laser focussing. The laser power was << 5 mW. Data were acquired in the 900 – 1800 Δcm^{-1} range with 600 l/mm spectral grating. Calibration involved the analysis of a silicon wafer with a distinctive 520 Δcm^{-1} band. The acquisition time was 15 s with 10 accumulations. Project Four (WITec GmbH) was used for background correction.

RESULTS

Texture, petrography, and chemistry of stromatolites and barite

The Dresser Formation sulfidized stromatolites analyzed here consist of wavy to gently undulating and wrinkly sulfide–dolomite laminae, as well as millimeter– to centimeter– scale sulfide–dolomite columns that exhibit microns–scale lamination (Fig. 2a; c.f., Baumgartner et al., 2019, 2020a). These well–preserved, strongly sulfidized stromatolite structures lie within centimeters–thick beds of chert and dolomite, but finely laminated stromatolite layers also occur within horizons of euhedral to subhedral, coarsely crystalline barite (plus minor quartz and dolomite) that are interlayered with the stromatolites (Fig. 2a–c; Fig. DR1 and DR2).

The stromatolites are primarily composed of organic matter–rich, nano–porous pyrite that is overgrown by a later generation of non–porous, massive pyrite; dolomite, quartz, and sphalerite are intergrown with these pyrite types (c.f., Baumgartner et al., 2019, 2020a). Element mapping by SR–XFM documents strong enrichments of Ni within pyrite of the stromatolites. This technique also reveals that stromatolitic sulfide laminae within barite generally continue across intrusive, anhedral to subhedral, barite macro–crystals, which generally show well–developed growth zonation and Sr enrichment (Fig. 2c–e; Fig. DR1).

Micro–mineralogy and chemistry of micro-spherulitic barite

High–resolution electron imaging of the sulfidized Dresser Formation stromatolites following nitric acid etching reveals the presence of generally submicron–scale, platy tabular to lenticular barite grains, and submicron–scale barite spherulites that are intimately associated with dolomite and organic

This article is protected by copyright. All rights reserved

Author Manuscript

matter–rich, nano–porous pyrite (Fig. 3a–f; Fig. DR3). The barite micro–spherulites show smooth– to rough–textured surfaces, as well as hollow to well–crystallized, irregular (framboid–like) to radiating, crystalline interiors (Fig. 3c–e; Fig. DR3a–c). Most barite micro–spherulites with well–crystallized cores exhibit unattached outer shells (e.g., Fig. 3c and d). Both the platy tabular/spherulitic barite morphotypes usually have narrow size distributions (i.e., ~0.3 to ~1 μm), but some localities in the samples have greater grain size variations and grains that are significantly smaller than 100 nm (e.g., Fig. 3a and f).

Some barite micro–spherulites have been pseudomorphed to pyrite, particularly at the contacts between sulfidized stromatolites and overlying, or underlying, coarse–grained barite layers (Fig. 4a; Fig. DR3d and DR4). Indeed, nitric acid etching reveals that some parts of the coarse–grained barite crystals that lie in proximity to stromatolite layers are actually composed of close–packed to intergrown agglomerations of micro–spherulitic barite (Fig. 4b; Fig. DR2; Fig. DR3e and f), whereas barite crystals located away from the stromatolite layers show homogeneous internal textures and well–developed growth zonations (Fig. DR1).

More than 40 chemical analyses (EDS) of barite micro–spherulites and platy tabular/lenticular barite reveal that they contain variable concentrations of Na, Mg, Al, Si, P, K, Ca and Sr (Fig. 5a). However, the small sizes of barite micro–spherulites precluded their accurate analysis and assessment of eventual relationships between barite chemistry and morphology. High–resolution electron imaging, EDS analysis, and Raman Spectroscopy analysis reveal that both barite morphotypes are ubiquitously associated with thermally mature, kerogen–like organic matter (Fig. 3a–f; Fig. 5; Fig. DR3c–d), including some notable examples where nanoscopic barite spherulites encrust clumps and coherent strands of organic matter (Fig. 3f). Complementary TEM–EDS analysis of a barite micro–spherulite assemblage resolves C enrichments in their interiors (Fig. 6).

DISCUSSION

Barite is a common mineral in Earth's crust and may be used as a proxy for the geological environment and the ambient conditions at the time of formation. For instance, barite in marine hydrothermal systems generally forms well–developed, tabular and bladed crystals, acicular/radiating tapered crystals, and/or dendritic crystals (e.g., Harris et al., 2009; Griffith and Paytan, 2012; Ray et al., 2014; Jamieson et al., 2016). On the other hand, barite in the water column and within pelagic sediment typically occurs as rounded, elliptical, or platy tabular grains (e.g., Dehairs et al., 1980; Bertram and James, 1997; Griffith and Paytan, 2012). Although the detailed factor(s) in the development of a specific barite morphotype are not entirely understood, laboratory experiments show that variations can be controlled by physical factors such as saturation index, crystal growth rate and temperature, as well

This article is protected by copyright. All rights reserved

Author Manuscript

as chemistry, especially the ratio of $Ba^{2+}/SO4^{2-}$ in solution, the presence/abundance of organic molecules, and the availability of ions that may substitute for Ba^{2+} in the crystal lattice (Mg^{2+}, Ca^{2+}, and Sr^{2+}; e.g., Smith et al., 2004; Judat and Kind, 2004; Jones et al., 2007; Kowacz et al., 2007; Godinho and Stack, 2015; Ruiz–Agudo et al., 2015; Widanagamage et al., 2018).

The incorporation of organic molecules, and perhaps Sr^{2+} cations into the crystal lattice of barite, plus organics promoting supersaturation and inhibiting crystal growth, are known to promote the development of both platy tabular/lenticular grains and polycrystalline barite aggregates with spherulitic shape (e.g., Smith et al., 2004; Jones et al., 2007; Widanagamage et al., 2018). The importance of organics in the formation of spherulitic barite is further demonstrated by experiments involving marine microbial cultures, which revealed that cellular surfaces and EPS can act as a nucleation site of spherulitic barite (Fig. 3g–h, and see additional data in González–Muñoz et al., 2012, Stevens et al., 2015, and Torres–Crespo et al., 2015). This observation, in addition to the fact that high concentrations of biomass/dissolved organic matter help in overcoming barite undersaturation (Goldberg and Arrhenius, 1958; Dehairs et al., 1980; Bertram and James, 1997; Horner et al., 2017; Martinez–Ruiz et al., 2018a, 2018b; Deng et al., 2019; among others), suggest that precipitation of spherulitic barite may be common in the pelagic zones of the oceans, such as at cold seeps where such mineralization have been found to occur in association with communities of sulfur–cycling microbes (Stevens et al., 2015).

Whereas microbial activity and/or the presence of degrading biomass can facilitate the formation of spherulitic barite aggregates, their sizes, as well as their detailed micro–textural and micro–mineralogical characteristics, may vary in relation to even subtle differences in ambient physical and chemical parameters during precipitation. For instance, laboratory experiments involving humic substances have produced framboid–like spherulitic agglomerations of euhedral barite nanocrystallites (Smith et al., 2004). On the other hand, microbial experiments by Torres–Crespo et al. (2015) have formed both densely crystalline spherulites and nano–scale hollow spheres with diameters in the <<1μm to >10 μm range (Fig. 3g), whereas biogenic barite precipitates in Gonzalez–Munoz et al. (2012) generally have consistent sizes and form radiating compact spherical clusters of acicular crystals (Fig. 3h). Importantly, the 3.48 billion–year–old barite micro–spherulites described in this study not only share several micro–textural features with these spherulitic barite types known from laboratory experiments and natural examples (compare Fig. 3a-f with Fig. 3g-h, and with additional data in Gonzalez–Munoz et al., 2012, Stevens et al., 2015, and Torres-Crespo et al., 2015), they also have poorly crystallized, in part nano–porous interiors that could indicate formation from amorphous

This article is protected by copyright. All rights reserved

Author Manuscript

precursors (compare Fig. 3d with Fig. 6 in Martinez–Ruiz et al., 2018b), and they contain trace concentrations of P (Fig. 5a), as is found in some biogenic barite examples.

An additional, critical observation in this study is that barite micro–spherulites are ubiquitously found in the earliest formed mineral assemblages that make up the Dresser Formation sulfidized stromatolites; ie., dolomite and nano–porous pyrite containing organic matter and enriched in various transition metals (e.g., Ni and Zn); Fig. 3a–f and Fig. DR3a–c; c.f., Baumgartner et al. (2019, 2020a). The texture and chemistry of this organic matter–rich, texturally distinctive nano–porous pyrite is consistent with an origin through sulfidization of biofilms as early as during stromatolite growth (c.f., Baumgartner et al., 2019, 2020a), as is supported by the presence of entombed, autochthonous organic matter strands and filaments that closely resemble variably degraded and remineralized EPS (compare the organic matter that is encrusted by barite micro–spherulites in Fig. 3f with organic matter strands in Baumgartner et al. [2019, their Fig. 4]). Hence, while all the physical and chemical factors that can control barite morphology are still not entirely understood (c.f., Widanagamage et al., 2018), our data suggest that intimately associated organics have been important factors for micro–spherulite formation. These organics were likely derived from (decaying) ancient microbial mats that flourished in a hydrothermally influenced, low–temperature, shallow water depositional environment (Nijman et al., 1998; Van Kranendonk and Pirajno, 2004; Van Kranendonk, 2006; Van Kranendonk et al., 2008, 2018; Djokic et al., 2017; among others). The barium and sulfate for precipitating barite may have been sourced from hydrothermal fluids and intermixed seawater (c.f., Philippot et al., 2007, 2012; Ueno et al., 2008; Shen et al., 2009; Baumgartner et al., 2020b). Living microbial communities and/or dead microbial biomass could have served as precipitation sites for micro–spherulitic barite, through direct formation on EPS, or promoted by strong chemical gradients established by degrading biomass and the presence of organic matter.

Interestingly, we note that spherulitic barite is also common in close vicinity to stromatolite layers within bedding–parallel, coarse–grained barite (Fig. 4b; Fig. DR3e and f). These large, euhedral to subhedral, strongly zoned barite crystals are similar to barite that typically forms in hydrothermal vein systems and marine hydrothermal vents (compare Fig. 2d and e and Fig. DR1 with Fig. 2 in Jamieson et al., 2016 A late–stage origin for the coarse–grained barite in the Dresser Formation sulfidized stromatolite samples studied here is indicated by the fact that some barite crystals have deformed, intruded into, and ripped apart some stromatolite laminae (Fig. 2c–e). By comparison, spherulitic barite within the sulfidized stromatolites is intimately associated with petrogenetically earliest dolomite and organic matter–rich, nano–porous pyrite. An early formation of micro–spherulitic barite is further supported by the fact that these mineralizations are locally pseudomorphed to pyrite

This article is protected by copyright. All rights reserved

Author Manuscript

(Figs. 4, DR3d), and clearly are overgrown by the coarse–grained barite crystals. Hence, these textural/petrographical relationships and the correspondent variations in barite morphology allow for detailed inferences on the temporal evolution of barite precipitation: 1) precipitation of the barite micro–spherulites in a low temperature regime, as early as during growth and sulfidization of the stromatolites; 2) precipitation of the coarse–grained barite crystals in relation to fluid percolation at some stage following demise and burial of the stromatolites.

CONCLUSION

Sulfidized stromatolites from the ~ 3.5 Ga Dresser Formation that contain abundant organic matter, including potential microbial remains (Baumgartner et al., 2019), host micro–spherulitic barite aggregates and platy tabular/lenticular barite grains. These barite morphotypes, which are associated with petrographically earliest dolomite and nano–porous pyrite enriched in autochthonous organic matter, show striking textural and chemical similarities with barite precipitates that are known to develop under low–temperature conditions in the presence of microbial activity or degrading biomass. This finding lends further support to a biogenic origin of the Dresser Formation stromatolites.

ACKNOWLEDGEMENTS

The authors acknowledge the facilities, and the scientific and technical assistance of the Microscopy Australia research facility at the Centre for Microscopy, Characterization and Analysis (UWA). This study was supported by the Australian Research Council (ARC) Centre of Excellence for Core to Crust Fluid Systems (www.ccfs.mq.edu.au). Additional support came from the University of New South Wales (Sydney), and ARC Discovery Project 180103204.

REFERENCES CITED

Baumgartner, R.J., Van Kranendonk, M.J., Wacey, D., Fiorentini, M.L., Saunders, M., Caruso, S., Pagès, A., Homann, M., Guagliardo, P. (2019) Nano−porous pyrite and organic matter in 3.5–billion–year–old stromatolites record primordial life. Geology, 47, 1039–1043.

Baumgartner, R.J., Van Kranendonk, M.J., Pagès, A., Fiorentini, M.L., Wacey, D., Ryan, C. (2020a) Accumulation of transition metals and metalloids in sulfidized stromatolites of the 3.48 billion–year–old Dresser Formation, Pilbara Craton. Precambrian Research, https://doi.org/10.1016/j.precamres.2019.105534.

Baumgartner, R.J., Caruso, S., Fiorentini, M.L., Van Kranendonk, M.J., Martin, L., Jeon, H., Pagès, A., Wacey, D. (2020b) Sulfidization of 3.48 billion-year-old stromatolites of the Dresser Formation, Pilbara Craton: Constraints from in-situ sulfur isotope analysis of pyrite. Chemical Geology, https://doi.org/10.1016/j.chemgeo.2020.119488.

This article is protected by copyright. All rights reserved

Author Manuscript

Bertram, M.A., James, P.C. (1997) Morphological and compositional evidence for biotic precipitation of marine barite. Journal of Marine Research, 55, 577–593.

Buick, R., Dunlop, J.S.R. (1990) Evaporitic sediments of Early Archaean age from the Warrawoona Group, North Pole, Western Australia: Sedimentology, 37, 247–277.

Buick, R., Dunlop, J.S.R., and Groves, D.I. (1981) Stromatolite recognition in ancient rocks: An appraisal of irregularly laminated structures in an Early Archaean chert–barite unit from North Pole, Western Australia: Alcheringa, 5, 161–181

Dehairs, F., Stroobants, N., Goeyens, L. (1991) Suspended barite as a tracer of biological activity in the Southern Ocean. Marine Chemistry, 35, 399–410.

Deng, N., Stack, A.G., Weber, J., Cao, B., De Yoreo, J.J., Hu, Y. (2019) Organic–mineral interfacial chemistry drives heterogeneous nucleation of Sr–rich $(Ba_x,Sr_{1-x})SO_4$ from undersaturated solution. Proceedings of the National Academy of Sciences of the United Stated of America, 116, 13221–13226.

Djokic, T., Van Kranendonk, M.J., Campbell, K.A., Walter, M.R., Ward, C.R. (2017) Earliest signs of life on land preserved in ca. 3.5 Ga hot spring deposits: Nature Communications, doi:10.1038/ncomms15263.

Duda, J.P., Thiel. V., Bauersachs, T., Miβbach, H., Reinhardt, M., Schäfer, N., Van Kranendonk, M.J., Reitner, J. (2018) Ideas and perspectives: hydrothermally driven redistribution and sequestration of early Archaean biomass – the "hydrothermal pump hypothesis. Biogeosciences, 15, 1535–1548.

Dunlop, J.S.R., Buick, R. (1981) Archaean epiclastic sediments derived from mafic volcanics, North Pole, Pilbara Block, Western Australia: Geological Society of Western Australia Special Publication, 7, 225–233.

Glikson, M., Duck, L.J., Golding, S.D., Hofmann, A., Bolhar, R., Webb, R., Baiano, J.C.F., Sly, L.I. (2008) Microbial remains in some earliest Earth rocks: Comparison with a potential modern analogue. Precambrian Research, 164, 187–200.

Godinho, J.R., Stack, A.G. (2015) Growth Kinetics morphology of barite crystals derived from face–specific growth rates. Crystal Growth & Design, 15, 2064–2071.

Goldberg, E.D., Arrhenius, G. (1958) Chemistry of pelagic sediments. Geochimica et Cosmochimica Acta 13, 153–212.

González–Muñoz, M.T., Fernández–Luque, P., Martínez–Ruiz, F., Ben Chekroun, P., Arias, J.M., Rodríguez–Gallego, M., M. Martínez–Cañamero, M., De Linares,, C., Paytan, A. (2003) Precipitation of barite by Myxococcus xanthus: possible implications for the biogeochemical cycle of barium. Applied and Environmental Microbiology, 69, 5722–5725.

This article is protected by copyright. All rights reserved

Author Manuscript

González–Muñoz, M.T., Martinez–Ruiz, F., Morcillo, F., Martin–Ramos, J.D., Paytan, A. (2012) Precipitation of barite by marine bacteria: A possible mechanism for marine barite formation. Geology 40, 675–678.

Griffith, E.M., Paytan, A. (2012) Barite in the ocean – occurrence, geochemistry and palaeoceanographic applications. Sedimentology, 59, 1817–1835.

Groves, D.I., Dunlop, J.S.R., and Buick, R. (1981) An early habitat of life. Scientific American, 245, 64–73.

Harris, A.C, White, N.C., McPhie, J., Bull, S.W., Line, M.A., Skrzeczynski, R., Mernagh, T.P., Tosdal, R.M. (2009) Early Archean Hot Springs above Epithermal Veins, North Pole, Western Australia: New Insights from Fluid Inclusion Microanalysis. Economic Geology, 104, 793–814.

Harris, L.V., Hutchinson, I.B., Ingley, R., Marshall, C.P., Olcott Marshall, O., and Edwards, H.G.M., (2015) Selection of portable spectrometers for planetary exploration: A comparison of 532 nm and 785 nm Raman Spectroscopy of reduced carbon in Archean cherts: Astrobiology, v. 15, p. 420–429, https://doi .org/10.1089/ast.2014.1220.

Horner, T.J., Pryer, H.V., Nielsen, S.G., Crockford, P.W., Gauglitz, J.M., Wing, B.A., Ricketts, R.D. (2017) Pelagic barite precipitation at micromolar ambient sulfate. Nature Communications, https://doi:10.1038/s41467–017–01229–5.

Jamieson, J.W., Hannington, M.D., Tivey, M.K., Hansteen, T., Williamson, N.M.–B., Stewart, M., Fietzke, J., Butterfield, D., Frische, M., Allen, L., Cousens, B., Langer, J (2016) Precipitation and growth of barite within hydrothermal vent deposits from the Endeavour Segment, Juan de Fuca Ridge. Geochimica et Cosmochimica Acta, 173, 64–85.

Jones, F., Jones, P., Ogden, M.I., Richmond, W.R., Rhol, A.I., Saunders, M. (2007) The interaction of EDTA with barium sulfate. Journal of Colloid and Interface Science, 316, 553–561.

Judat, B., Kind, M. (2004) Morphology and internal structure of barium sulfate—Derivation of a new growth mechanism. Journal of Colloid and Interface Science, 269, 341–353.

Kowacz, M., Putnis, C.V., Putnis, A. (2007) The effect of cation:anion ratio in solution on the mechanism of Barite growth at constant supersaturation: Role of desolvation on the growth kinetics. Geochim. Cosmochim. Acta, 71, 5168–5179.

Martinez–Ruiz, F., Jroundi, F., Paytan, A., Guerra–Tschuschke, I., Del Mar Abad, M.M., González–Muñoz, M.T. (2018a) Barium bioaccumulation by bacterial biofilms and implications for Ba cycling and use of Ba proxies. Nature Communications, https://doi:10.1038/s41467–018–04069–z.

This article is protected by copyright. All rights reserved

Author Manuscript

Martinez–Ruiz, F., Paytan, A., González–Muñoz, M.T., Jroundi, F., Abad, M.M., Lam, P.J., Bishop, J.K.P., Horner, T.J., Morton, P.L., Kastner, M. (2018b) Barite formation in the ocean: Origin of amorphous and crystalline precipitates. Chemical Geology, 511, 441–451.

Morag, N., Williford, K. H., Kitajima, K., Philippot, P., Van Kranendonk, M.J., Lepot, K., Thomazo, C., Valley, J.V. (2016) Microstructure–specific carbon isotopic signatures of organic matter from ~3.5 Ga cherts of the Pilbara Craton support a biologic origin: Precambrian Research, 275, 429–449.

Nijman, W., De Bruin, K., Valkering, M. (1998) Growth fault control of early Archaean cherts, barite mounds, and chert–barite veins, North Pole Dome, Eastern Pilbara, Western Australia. Precambrian Research, 88, 25–52.

Paterson, D., De Jonge, M.D., Howard, D.L., Lewis, W., McKinlay, J., Starritt, A., Kusel, M., Ryan, C.G., Kirkham, R., Moorhead, G., Siddons, P. (2011) The X–ray Fluorescence Microscopy Beamline at the Australian Synchrotron. AIP Conference Proceedings, 1365, 219–222.

Philippot, P., Van Zuilen, M., Lepot, K., Thomazo, C., Farquhar, J., Van Kranendonk, M.J. (2007) Early Archean microorganisms preferred elemental sulphur, not sulphate. Science, 317, 1534–1537.

Philippot, P., Van Zuilen, M., Rollion-Bard (2012) Variations in atmospheric sulphur chemistry on early Earth linked to volcanic activity. Nature Geoscience, 5, 668–674.

Pirajno, F., Van Kranendonk, M.J. (2005) A review of hydrothermal processes and systems on earth and implications for Martian analogues. Australian Journal of Earth Sciences, 52, 329–351.

Ray, D., Kota, D., Das, P., Surya Prakash, L., Khedekar, V.D. (2014) Microtexture and distribution of minerals in hydrothermal Barite–silica chimney from the Franklin seamount, SW Pacific: Constraints on mode of formation. Acta Geolica Sinica, 88, 213–225.

Ruiz–Agudo, C., Putnis, C.V., Ruiz–Agudo, E., Putnis, A. (2015) The influence of pH on barite nucleation and growth. Chemical Geology, 391, 7–18.

Runnegar, B., Dollase, W. A., Ketcham, R.A., Colbert, M., Carlson, W.D. (2001) Early Archaean sulphates from Western Australia first formed as hydrothermal barite not gypsum evaporites. Geological Society of America Abstracts, 33, A–404.

Ryan, C.G., Siddons, D.P., Kirkham, R., Dunn, P.A., Kuczewski, A., Moorhead, G., De Geronimo, G., Paterson, D.J., de Jonge, M.D., Hough, R.M., Lintern, M.J., Howard, D.L., Kappen, P., Cleverley, J., Denecke, M., Walker, C.T. (2010) The New Maia Detector System: methods for high definition trace element imaging of natural material. AIP Conference Proceedings, 1221, 9–17.

This article is protected by copyright. All rights reserved

Author Manuscript

Shen, Y., Buick, R., Canfield, D.E. (2001) Isotopic evidence for microbial sulphate reduction in the early Archaean era. Nature, 410, 77–81.

Shen, Y.N., Farquhar, J., Masterson, A., Kaufman, A.J, Buick, R. (2009) Evaluating the role of microbial sulfate reduction in the early Archean using quadruple sulfur isotope systematics. Earth and Planetary Science Letters, 279, 383–391.

Smith, E., Hamilton–Taylor, J., Davison, W., Fullwood, N.J., McGrath, M. (2004) The effect of humic substances on barite precipitation–dissolution behaviour in natural and synthetic lake waters. Chemical Geology, 207, 81–89.

Stevens, E.W.N., Bailey, J.V., Flood, B.E., Jones, D.S., Gilhooly, W.P., Joye, S.B., Teske, A., Mason, O.U. (2015) Barite encrustation of benthic sulfur–oxidizing bacteria at a marine cold seep. Geobiology, 13, 588–603.

Torres–Crespo, N., Martinez–Ruiz, F., González–Muñoz, M.T., Bedmar, E.J., De Lange, G.J., Jroundi, F. (2015) Role of bacteria in marine barite precipitation: A case using Mediterranean seawater. Science of the Total Environment, 512–513, 562–571.

Ueno, Y., Isozaki, H., Yurimoto, H., Maruyama, S. (2001) Carbon isotopic signatures of individual Archean microfossils (?) from Western Australia. International Geology Reviews, 43, 196–212.

Ueno, Y., Ono, S., Rumble, D., Maruyama, S. (2008) Quadruple sulfur isotope analysis of ca. 3.5 Ga Dresser Formation: New evidence for microbial sulfate reduction in the early Archean. Geochimica et Cosmochimica Acta, 72, 5675–5691.

Ueno, Y., Yamada, K., Yoshida, N., Maruyama, S., Isozaki, Y. (2006) Evidence from fluid inclusions for microbial methanogenesis in the early Archaean era. Nature, 440, 516–519.

Van Kranendonk, M.., Hickman, A.H., Williams, I.R., Nijman, W. (2001) Archaean geology of the East Pilbara Granite–Greenstone Terrane, Western Australia – a field guide. Western Australia Geological Survey, Record 2001/9, p. 134.

Van Kranendonk, M.J. (2006) Volcanic degassing, hydrothermal circulation and the flourishing of early life on Earth: new evidence from the Warrawoona Group, Pilbara Craton, Western Australia. Earth Science Reviews, 74, 197–240.

Van Kranendonk, M.J. (2011) Morphology as an indictor of biogenicity for 3.5–3.2 Ga Fossil stromatolites from the Pilbara Craton, Western Australia: Lecture Notes in Earth Sciences, 131, 537–554.

Van Kranendonk, M.J., Djokic, T., Poole, G., Tadbiri, S., Steller, L., Baumgartner, R. (2018) Depositional setting of the fossiliferous, c. 3480 Ma Dresser Formation, Pilbara Craton: A review.

This article is protected by copyright. All rights reserved

Author Manuscript

In: Van Kranendonk, M.J., Bennett, V., Hoffmann, E. (eds.), Earth's Oldest Rocks, 2nd Edition. Elsevier, USA; p. 985–1006.

Van Kranendonk, M.J., Philippot, P., Lepot, K., Bodorkos, S., Pirajno, F. (2008) Geological setting of Earth's oldest fossils in the ca. 3.5 Ga Dresser Formation, Pilbara Craton, Western Australia: Precambrian Research, 167, 93–124.

Van Kranendonk, M.J., Pirajno, F. (2004) Geochemistry of metabasalts and hydrothermal alteration zones associated with c. 3.45 Ga chert and barite deposits: implications for the geological setting of the Warrawoona Group, Pilbara Craton, Australia: Geochemistry: Exploration, Environment, Analysis, 4, 253–278.

Van Kranendonk, M.J., Smithies, R.H., Hickman, A.H., Champion, D.C. (2007) Secular tectonic evolution of Archaean continental crust: interplay between horizontal and vertical processes in the formation of the Pilbara Craton, Australia. Terra Nova, 19, 1–38.

Walter, M.R., Buick, R., Dunlop, J.S.R (1980) Stromatolites 3,400–3,500 Myr old from the North Pole area, Western Australia. Nature, 284, 443–445.

Widanagamage, I.H., Waldron, A.R., Glamoclija, M. (2018) Controls on barite crystal morphology during abiotic precipitation. Minerals, 8, 480.

FIGURE CAPTIONS

Figure 1. Geology at North Pole Dome, Pilbara Craton, Western Australia, and location of the stromatolites within the drill core examined in this study. a) Geology at North Pole Dome, where the red circle indicates the location of the PDP2b drilling site (redrawn after Van Kranendonk et al., 2008; see also Baumgartner et al. 2019, 2020b). b) Stratigraphy of the PDP2b drillcore, where the red circle indicates the stratigraphic position of the here examined sulfidized stromatolites (image taken from Baumgartner et al., 2019).

Figure 2. SEM images and SR–XFM element maps of pyritized stromatolites and interlayered barite. a–c) Backscattered Electron (BSE) images of pyritized, micro–laminated and columnar stromatolites (indicated by red arrows and dashed lines) in chert plus dolomite and interlayered barite. Image (a) and (b) are taken from Baumgartner et al. (2019). Note in (c) the barite crystal that intrudes and deforms a stromatolite lamina. Mineralogy is gauged from brightness differences and supported by Energy Dispersive X–ray Spectroscopy analysis: white = barite; light grey = sulfide; dark grey = chert and dolomite. d–e) BSE image and SR–XFM element map with color–grading of Ni (red), Ca (green) and Sr (blue), showing a pyritized stromatolite lamina – indicated in (e) by Ni – that is cut by coarsely crystalline barite –indicated in (e) by Sr. Note the alignment of sulfide inclusions parallel to the growth

This article is protected by copyright. All rights reserved

Author Manuscript

455 zonations of barite (black and white arrows), and the large, subhedral barite crystals that cut into the
456 base of the stromatolite lamina (red arrows).
457 Figure 3. SEM and STEM images of micro–spherulitic barite from the Dresser Formation
458 stromatolites, and compared with modern analogues. a) Backscattered Electron (BSE) image of platy
459 tabular to lenticular barite (Brt) that occurs in association with dolomite (Dol) and pyrite (Py) of the
460 sulfidized stromatolites. b) Platy tabular to lenticular barite grains embedded within nano–porous pyrite
461 (red arrow) and organic matter (Om) c) Assemblage of micro–spherulitic barite and organic matter.
462 The white arrow indicates nano–porous pyrite enriched in organic matter. The arrow in the inset
463 indicates the outer shell of a barite micro–spherulite. The asterisk indicates the location of Raman
464 Spectroscopy analysis of organic matter (Fig. 5b). d) Dark–field STEM image showing the poorly
465 crystallized, to irregular or radiating crystalline interiors of some barite micro–spherulites (arrows from
466 left to right, respectively). See their chemical analysis in Fig. 6. e) Smooth–surfaced barite micro–
467 spherulites in dolomite (Dol). The image of the inset was taken at relatively higher acceleration voltage
468 (5 kV versus 20 kV). It indicates the partially hollow to entirely nano–crystalline interiors of the
469 spherulites. f) Barite micro–spherulites encrusting a coherent organic matter strand. The red arrows
470 indicate nano–porous pyrite and associated organic matter. g–h) Spherulitic barite of laboratory
471 experiments using marine microbes. The images are taken from Torres–Crespo et al. (2015) and
472 González–Muñoz et al. (2012), respectively. The inset in (g) shows the hollow interiors (red arrow) of
473 precipitating barite micro–spherulites; compare with (e) in this figure panel. Note in (h) the radiating
474 crystalline microtexture (red arrow) of spherulites. Images in (a–f) were acquired on nitric acid–etched
475 surfaces. See the imaging locations in Fig. DR2.
476 Figure 4. Backscattered Electron (BSE) images of micro–spherulitic pyrite (a) and micro–spherulitic
477 barite (b) at contacts between stromatolite laminae and layers of coarsely crystalline barite. Chemical
478 analysis of micro–spherulitic pyrite in (a) is shown in Fig. DR4. Note in (b) the range of textures from
479 closely packed micro–spherulites (left red arrow), to intergrown, globular agglomerations of micro–
480 spherulites (right red arrow). See imaging locations in Fig. DR2. Brt = barite; Om = organic matter; Py
481 = pyrite.
482 Figure 5. Chemical analysis of micro–spherulitic barite and Raman Spectroscopy analysis of associated
483 organic matter. a) Energy Dispersive X–ray Spectroscopy analyses of spherulitic barite. The green
484 spectrum is from platy tabular/lenticular barite in Fig. 3a. The black and pink spectra are from barite
485 spherulites in Fig. 3c. The grey spectrum is from barite micro–spherulites in Fig. DR3b and c. Note the
486 overlaps of Si and Sr peaks, and the small but distinctive peaks of P at ~ 2.0 keV. In the absence of
487 strong Ca and Mg peaks relating to carbonates (e.g., green EDS spectrum of platy tabular/lenticular

This article is protected by copyright. All rights reserved

Author Manuscript

barite shown in Fig. 3a), carbon peaks presumably relate to organic matter. The signals of S and Fe at least partially relate to the co–analysis of pyrite. b) Raman Spectroscopy analysis of organic matter using a 785 nm laser (see Methods). Analysis location is indicated in Fig. 3c.The high intensity of the disorder–induced 'D' band (~1315 Δcm^{-1}) relative to the order–induced 'G' band (~1600 Δcm^{-1}) is typical for thermally mature organic matter in the Dresser Formation; compare with Raman Spectroscopy analyses of Dresser Formation organic matter using a 785 nm laser in Harris et al. (2015) and in Baumgartner et al. (2019, 2020a).

Figure 6. STEM images and elemental distribution maps of barite micro–spherulites in sulfide of the Dresser Formation stromatolites. a–b) Dark–field STEM and bright–field STEM images of a milled cross section through barite micro–spherulites. The homogeneous material around the spherulites is Pt from sample preparation by Focused Ion Beam (FIB) milling. c–e) Energy Dispersive X–ray Spectroscopy element maps showing the distributions of Ba, O, and C, respectively. Platinum (blue) and Ga (red) are contamination from FIB milling. Note the thin shells around (white arrows), and the concentric enrichment of C (red arrow) within, the barite micro–spherulites. The FIB wafer was prepared following nitric acid etching, which strongly dissolved pyrite but left barite essentially unaffected. The lack of Pt within the spherulites indicates that the enrichments of C are original and not the result of contamination relating to Pt (re–) deposition during FIB milling. Ba = barite; Pt = platinum; Py = pyrite.

Author Manuscript

This article is protected by copyright. All rights reserved

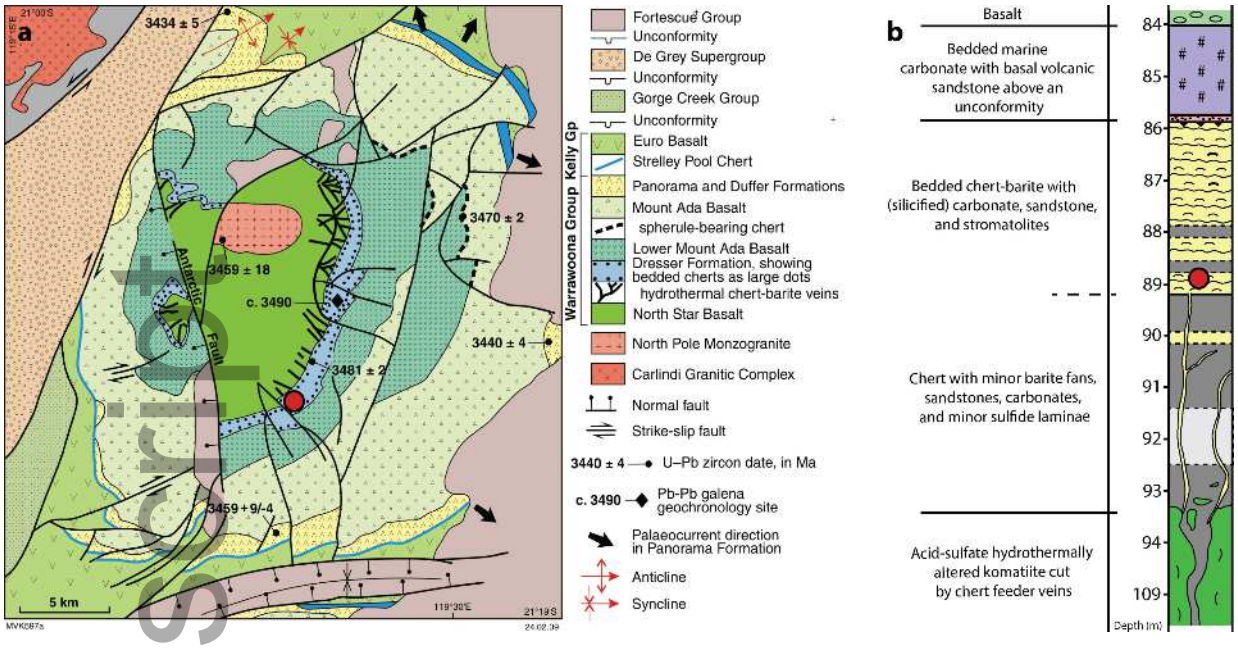

gbi_12392_f1.tif

Author Manuscript

This article is protected by copyright. All rights reserved

Author Manuscript

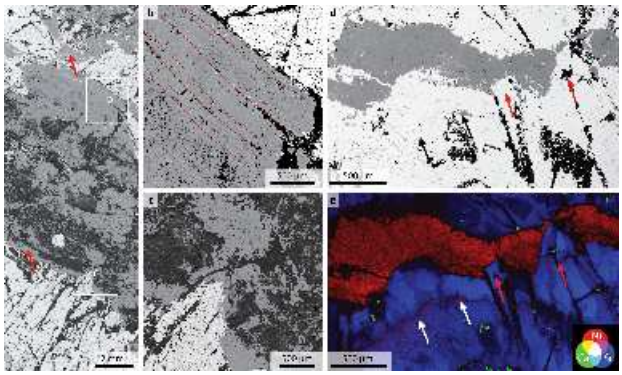

gbi_12392_f2.tif

This article is protected by copyright. All rights reserved

Author Manuscript

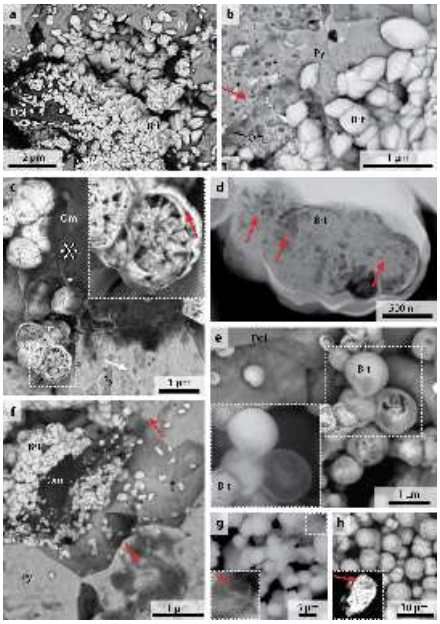

gbi_12392_f3.tif

This article is protected by copyright. All rights reserved

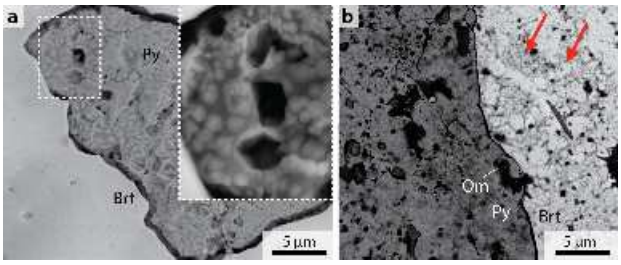

gbi_12392_f4.tif

Author Manuscript

This article is protected by copyright. All rights reserved

Author Manuscript

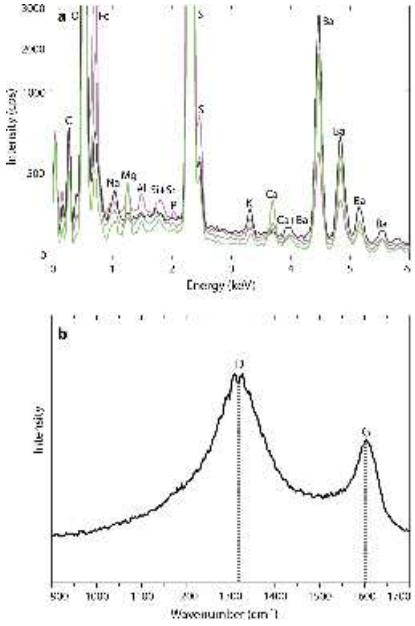

gbi_12392_f5.tif

This article is protected by copyright. All rights reserved

Author Manuscript

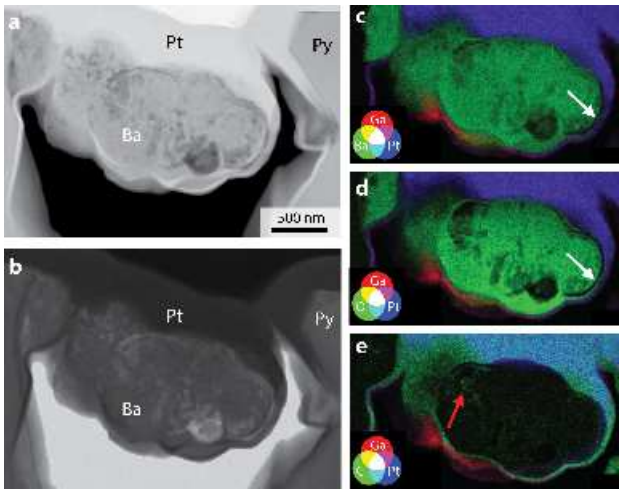

gbi_12392_f6.tif

This article is protected by copyright. All rights reserved